

# Antimatter cosmic rays from dark matter annihilation: First results from an N-body experiment

J. Lavalle,<sup>1</sup> E. Nezri,<sup>2</sup> F.-S. Ling,<sup>3</sup> E. Athanassoula,<sup>2</sup> and R. Teyssier<sup>4</sup>

<sup>1</sup>*Dipartimento di Fisica Teorica, Università di Torino - INFN, via Giuria 1, 10125 Torino - Italia\**

<sup>2</sup>*Laboratoire d'Astrophysique de Marseille, CNRS - Université Aix-Marseille I,  
2 place le Verrier, 13248 Marseille Cedex 4 - France<sup>†</sup>*

<sup>3</sup>*Service de Physique Théorique, Université Libre de Bruxelles,  
boulevard du Triomphe - CP225, 1050 Bruxelles - Belgique<sup>‡</sup>*

<sup>4</sup>*Service d'Astrophysique, Commissariat à l'Énergie Atomique, Orme des Merisiers, 91191 Gif sur Yvette<sup>§</sup>*

While the particle hypothesis for dark matter may be very soon investigated at the LHC, and as the PAMELA and GLAST satellites are currently taking new data on charged and gamma cosmic rays, the need of controlling the theoretical uncertainties affecting the possible indirect signatures of dark matter annihilation is of paramount importance. The uncertainties which originate from the dark matter distribution are difficult to estimate because current astrophysical observations provide rather weak dynamical constraints, and because, according to the results of cosmological N-body simulations, dark matter is neither smoothly nor spherically distributed in galactic halos. Some previous studies made use of N-body simulations to compute the gamma-ray flux from dark matter annihilation, but such a work has never been performed for the antimatter (positron and antiproton) primary fluxes, for which transport processes complicate the calculations. We take advantage of the galaxy-like 3D dark matter map extracted from the HORIZON Project results to calculate the positron and antiproton fluxes from dark matter annihilation, in a model-independent approach as well as for dark matter particle benchmarks relevant at the LHC scale (from supersymmetric and extra-dimensional theories). We find that the flux uncertainties arise mainly from fluctuations of the local density of dark matter, and are of about 1 order of magnitude. Though the spatial resolution of our N-body data is limited to  $\sim 200$  pc, our results are a first quantitative attempt with antimatter signals. We compare them to those obtained with analytic descriptions of the dark matter halo, showing that the latter may well reproduce the former. Finally, we stress the limits of the use of an N-body framework in this context.

PACS numbers: .....

DFTT-21/2008

## I. INTRODUCTION

The idea that dark matter is made of exotic weakly interacting massive particles (WIMP) is very appealing in the sense that the related existing frameworks in particle physics beyond the standard model (BSM) could solve (i) problems inherent to elementary particle theory, e.g. the force unification scheme and/or the stabilization of the theory against quantum corrections, which would thus confer a more fundamental meaning to this theory; and in the sametime (ii) the dark matter issue as characterized in astrophysics and cosmology (see e.g. [1] for a recent review). Indeed, the cold dark matter (CDM) paradigm seems to feature a powerful and self-consistent theory of structure formation, which at present is able to reproduce and explain most of large and mid scale observations (see e.g. [2] and references therein).

While the Large Hadron Collider at CERN (LHC) is about to start hunting BSM physics and may soon provide new insights about the dark matter particle hypothesis, high energy astrophysics experiments are also of strong interest to try to determine the actual nature of dark matter. Indeed, if dark matter is made of self-annihilating particles, a property which is found in many BSM models and which provides a natural mechanism to explain the dark matter cosmological abundance as observed today, there should be traces of annihilations imprinting the cosmic ray spectra (indirect detection of dark matter, see e.g. [3, 4, 5, 6]). Therefore, satellite experiments such as PAMELA and GLAST, which are dedicated to large field of view observations of charged cosmic rays and gamma-rays, respectively, in the MeV-TeV energy range, should be able to yield additional constraints or smoking guns very soon in this research field [7]. The most promising astrophysical messengers that could trace the annihilation processes are indeed gamma-rays and antimatter cosmic rays, which have been first investigated in [8] and in [9] respectively. Confinement and diffusion on magnetic turbulences limit the origin of the latter to our Galaxy, whereas the former, which only experiences the common  $r^{-2}$  flux dilution, may be observed even when emitted from extra-galactic regions.

Nevertheless, predictions of annihilation signals are affected by many uncertainties coming from (i) the under-

\*Electronic address: lavalle@to.infn.it

<sup>†</sup>Electronic address: Emmanuel.Nezri@oamp.fr, lia@oamp.fr

<sup>‡</sup>Electronic address: fling@ulb.ac.be

<sup>§</sup>Electronic address: romain.teyssier@cea.fr

lying WIMP model (ii) the distribution of dark matter in the relevant sources (iii) the propagation of charged cosmic rays in the Galaxy in the case of searches in the antimatter cosmic ray spectra. The first point is encoded in the WIMP mass, the annihilation cross-section and the annihilation final states which fully define the injected cosmic ray spectra: this has been widely investigated for years. The second point is currently surveyed by the state-of-the-art N-body experiments, but the use of N-body dark matter maps in the context of indirect detection has only been performed for gamma-ray predictions [10, 11, 12, 13]. Besides, there has been lots of efforts to estimate the effect of varying the dark matter distribution by means of analytical calculations, allowing for instance to study the effects of sub-halos on the gamma-ray [14, 15, 16, 17, 18] as well as on the antimatter primary fluxes [19, 20]. Such analytical studies mostly rely on the statistical information supplied by N-body simulations. However, though they provide very nice theoretical bases to unveil the salient effects of any change in the physical parameters, and permit to go beyond the current numerical resolution limits, they are usually bound to simplifying hypotheses, such as the sphericity of sources. Especially, no study of the antimatter signatures has been performed in the frame of N-body environments up to now. Finally, point (iii), referring to cosmic ray propagation, has also widely been investigated for antiprotons [21, 22] and positrons [20, 23], and while the transport processes depend on sets of still degenerate parameters within different propagation models, the origins of uncertainties are now rather well understood.

In this paper, we make use of a realistic (in the sense of  $\Lambda$ CDM cosmology) 3D dark matter distribution of a galactic-sized halo extracted from the HORIZON Project simulation results to study the antimatter signals. Our main purposes are to characterize and quantify the uncertainties coming from dark matter inhomogeneities (not necessarily clumps) and departure from spherical symmetry in a virialized Milky-Way-like object; and finally make predictions for different dark matter particle candidates. Despite the rather low resolution of our numerical data compared with the highest-level artillery on the market, as portrayed, e.g., by the Via Lactea simulations [11, 24], we study for the first time the production of antimatter cosmic rays from dark matter annihilation in an N-body framework. The resolution issue is however less important for charged cosmic rays than for gamma-rays, because the signal is strongly diluted by diffusion effects, which therefore tends to smooth the effects of high density gradients. Nevertheless, as very local density fluctuations are expected to affect the antimatter signals, we will quantify the effect of the lack of resolution by analytically extrapolating our results. For the WIMP candidates, we will use a model-independent approach as well as typical models of BSM theories, some of them being observable at the LHC.

This article is parted as follows: we recall the salient features of the HORIZON N-body experiment in Sect. II;

then, in Sect. III, we briefly review the positron and antiproton propagation before sketching the method we adopt to connect the propagation to the N-body source terms; we describe the WIMP models in Sect. IV; we finally present and discuss our results in Sect. V (where the expert reader is invited to go directly) before concluding.

## II. THE HORIZON FRAMEWORK

The framework of this study is a simulation of the Horizon collaboration. The run used the Adaptive Mesh Refinement code RAMSES [25] with an effective number of particles of  $N_p = 1024^3$  in a box of size  $L = 20h^{-1}$  Mpc where the initial conditions were fixed by the WMAP3 results ( $\Omega_m = 0.24$ ,  $\Omega_\Lambda = 0.76$ ,  $\Omega_b = 0.042$ ,  $n = 0.958$ ,  $H_0 = 73$ ,  $\sigma_8 = 0.77$ ).

A Milky-Way sized halo at  $z = 0$  was selected and refined using the so-called “zoom” technique. We obtained a maximum linear resolution of about 200 pc and the particle mass is  $M_p = 7.46 \cdot 10^5$  in solar mass ( $M_\odot$ ) units (we refer the reader to ref. [12] for more details on the characteristics and the analysis of the simulation.).

A non biased calculation of the dark matter density around a simulation point  $i$  is given by the algorithm of Casertano and Hut [26], namely:

$$\rho_j^i = \frac{j-1}{V(r_j)} M_p ; \quad (1)$$

where  $V(r_j) = 4\pi/3 r_j^3$  is the volume of the smallest sphere around the particle  $i$  that includes  $j$  neighbors.

The virial radius (defined as  $\rho(r_{vir}) = 200\rho_c$ ) of our halo is equal to 253 kpc, corresponding to an enclosed mass of  $6.05 \times 10^{11} M_\odot$  or  $8.1 \times 10^5$  particles. Within this radius, the dark matter halo density can be fitted by the usual spherical parameterization:

$$\rho(r) = \rho_0 \left( \frac{r}{r_0} \right)^{-\gamma} \left[ \frac{1 + (r_0/a)^\alpha}{1 + (r/a)^\alpha} \right]^{\frac{\beta-\gamma}{\alpha}}, \quad (2)$$

where  $\rho_0 = \rho_\odot$  is the local density in the solar neighborhood and  $r_0 = R_\odot = 8$  kpc is the distance from the Sun to the Galactic center (GC). Density maps, after projections in the  $(x, y)$  and  $(z, x)$  planes, are shown on Fig. 1, where the Earth has been located at three different positions: at  $x = 8$ ,  $y = 8$  and  $z = 8$  kpc, respectively (see Sect. IIIB for further details). When considering the radial distribution of our data, the best fit gives  $(\alpha, \beta, \gamma) = (0.39, 3.72, 0.254)$ , and  $a = 13.16$  kpc, but a NFW-like profile  $(1, 3, 1) - (a = 10 \text{ kpc})$  and a cored profile  $(0.5, 3.3, 0) - (a = 4.5 \text{ kpc})$  are also in good statistical agreement due to the resolution limits, especially in the central region. The averaged density at a radius of 8 kpc is  $\rho_\odot = 0.25 \pm 0.19 \text{ GeV/cm}^3$ . 108 sub-halos have been identified with masses between  $2 \times 10^7 M_\odot$  and  $2.4 \times 10^{10} M_\odot$  with a mass distribution following  $N(M_{sub}) \propto M_{sub}^{-1}$  above  $5 \times 10^8 M_\odot$ . Inside those substructures, the dark matter density scales like a universal

power law  $\rho_{cl}(r) \propto r^{-2.5}$  for the outer part. Regarding the inner part, the logarithmic slope is highly speculative due to the resolution limit. Furthermore, all clumps are found to be rather far from the Galactic center and will actually not modify our coming results. Anyway, though we will further mimic higher resolutions thanks to analytical extrapolations, this N-body environment is still relevant for the punch line of this study, which is to quantify the importance of solar neighborhood dark matter density fluctuations.

---

For charged Galactic cosmic rays in the GeV-TeV regime, the relevant (steady state) propagation equation which characterizes the transport, for any species, of the cosmic ray number density per unit of energy  $\mathcal{N}_{cr} \equiv dn_{cr}(E)/dE$  reads:

$$\vec{\nabla} \left[ K(E) \vec{\nabla} \mathcal{N}_{cr} - \vec{V}_{conv} \mathcal{N}_{cr} \right] + \frac{\partial}{\partial E} \left[ b(E) \mathcal{N}_{cr} + K_{EE} \frac{\partial}{\partial E} \mathcal{N}_{cr} \right] + \Gamma(E) \mathcal{N}_{cr} + \mathcal{Q} = 0 ; \quad (3)$$

where  $K(E)$  encodes the spatial diffusion due to scattering off magnetic turbulences,  $V_{conv}$  is the velocity of the convective wind that drifts cosmic rays out of the Galactic disk,  $b(E)$  stands for energy losses,  $K_{EE}$  characterizes diffusion in momentum space,  $\Gamma(E)$  features the spallation reactions and  $\mathcal{Q}$  is the (stationary) cosmic ray source of interest.

Though the above equation stands for any cosmic ray species, some of the processes can be safely neglected in the GeV regime, depending on the species. For positrons, the main processes are spatial diffusion and energy losses, so that we will neglect convection and reacceleration. Such an approximation is very often used in the literature, and its relevance is explained in great details in [27]. For antiprotons, the dominant processes beside diffusion are convection and spallation, which are more efficient at low energies, typically  $\lesssim 10$  GeV, whereas reacceleration and energy losses do not play a major role [21, 28]. We will therefore neglect those latter effects for antiprotons in the following.

The diffusion equation can be solved either fully numerically (see e.g. [29]) or semi-analytically in typical energy regimes and/or geometries of the diffusion zone (see e.g. [30]). We will use the latter approach in this paper. Generic solutions for point-like sources  $\propto \delta^4(E_S, \vec{x}_S)$  (4-D Dirac function) can be expressed in terms of Green functions  $\mathcal{G}(E, \vec{x}_\odot \leftarrow E_S, \vec{x}_S)$  that characterize the probability for cosmic rays of energy  $E_S$  injected at position  $\vec{x}_S$  to be detected at the Earth with energy  $E$ . Hence, for a WIMP particle of mass  $m_\chi$  and of thermally averaged annihilation cross-section  $\langle \sigma_{ann} v \rangle$ , the primary exotic flux at the Earth is merely given by:

$$\frac{d\phi_{cr}(E)}{dE} \equiv \frac{v_{cr}}{4\pi} \times \mathcal{S} \times \int_{slab} d^3\vec{x}_S \tilde{\mathcal{G}}(E; \vec{x}_\odot \leftarrow \vec{x}_S) \times \mathcal{Q}(\vec{x}_S), \quad (4)$$

where  $v_{cr}$  is the cosmic ray velocity,  $\mathcal{S} \equiv (\langle \sigma_{ann} v \rangle / 2) \times (\rho_\odot / m_\chi)^2$  allows a convenient normalization to the local WIMP-annihilation rate,  $\mathcal{Q}$  is the spatial source

### III. ANTIMATTER COSMIC RAYS

Antimatter cosmic rays are very interesting messengers to look for dark matter annihilation traces, because they are seldom produced in standard astrophysical processes. The astrophysical secondary background at the Earth is generically created out of the spallation of cosmic rays off the interstellar medium (ISM), and is expected to be highly power-law suppressed at energies above  $\sim 10$  GeV.

---

term that we will further discuss in Sect. IIIB, and  $\tilde{\mathcal{G}} \equiv \int dE_S \mathcal{G} dN/dE_S$  is the Green function convoluted with the injected cosmic ray spectrum  $dN/dE_S$ .

In the following, we present the main features of our propagation model for both antiprotons and positrons. We will end this section by discussing the source term  $\mathcal{Q}$  as set in our N-body framework.

#### A. Propagation model

The propagation model that we adopt in this paper is characterized by a slab geometry with the origin located at the Galactic center, a radial extent  $R_{slab}$  and a vertical half-height  $L$ . This defines the cosmic ray confinement zone (see Fig. 1), thanks to which we impose Dirichlet boundary conditions to Eq.(3), that is  $\mathcal{N}(R_{slab}, z) = \mathcal{N}(r, L) = 0$ . The Earth is located on a circle in the Galactic disc with cylindrical coordinates  $(r, z) = (8, 0)$  kpc (the polar angle is left free for the moment). As regards the transport processes, we take a spatial independent diffusion coefficient of the form  $K(E) = \beta K_0 \mathcal{R}^\delta$  (where  $\beta$  and  $\mathcal{R} = pc/Ze$  are the particle velocity and rigidity respectively) and a constant wind  $V_{conv}$  directed outwards the Galactic plane along the vertical  $z$  axis. The reader is referred to [31] for a detailed presentation of this framework. The propagation parameters can be constrained with cosmic ray measurements of secondary to primary ratios, and are found to be degenerate [31, 32, 33]. Throughout this paper, we will use the *median* set of propagation parameters defined in [21], which has been constrained with the current B/C data and which is recalled in Tab. I. Once the fluxes will be computed, they will be modulated to account for the so-

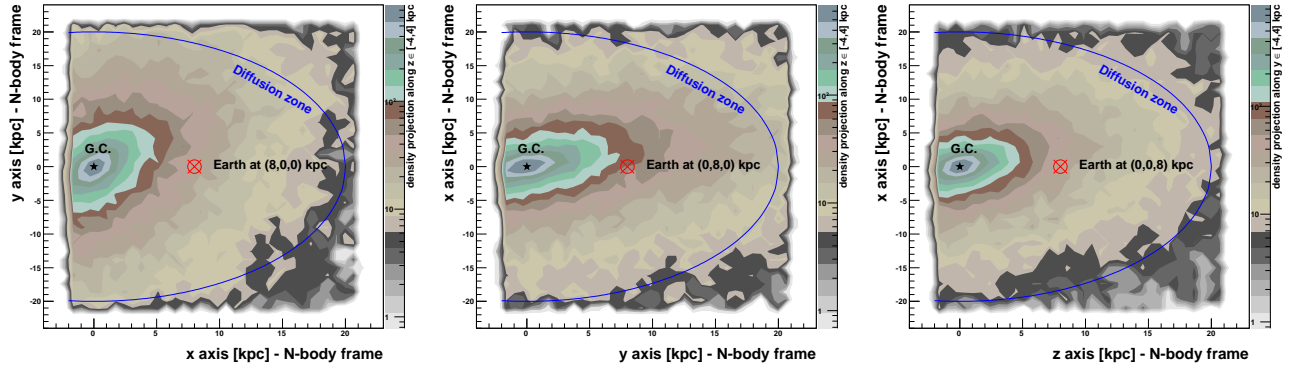


Figure 1: Projected dark matter density in the cosmic ray diffusion plane, for different choices of the Earth location (Cartesian coordinates). Left: Earth at  $x = 8$  kpc ( $\rho_\odot = 0.23 \text{ GeV.cm}^{-3}$ ), diffusion plane in  $Oxy$ ; middle: Earth at  $y = 8$  kpc ( $\rho_\odot = 0.28 \text{ GeV.cm}^{-3}$ ), diffusion plane in  $Oxy$ ; right: Earth at  $z = 8$  kpc ( $\rho_\odot = 0.13 \text{ GeV.cm}^{-3}$ ), diffusion zone in  $Oxz$ . The diffusion slab contour is explicitly drawn (visually ellipsoidal instead of spherical due to different horizontal and vertical scales).

$\delta$	$K_0$ ( $\text{kpc}^2.\text{Myr}^{-1}$ )	$L$ (kpc)	$R_{\text{slab}}$ (kpc)	$V_{\text{conv}}$ ( $\text{km.s}^{-1}$ )
med 0.70	0.0112	4	20	12.0

Table I: Propagation parameters compatible with B/C data giving the median antiproton primary (from dark matter annihilation) fluxes ; from [21].

lar modulation. We will use the force field approximation method, with an electric potential  $\phi = 600 \text{ MV}$  [34].

### 1. Antiproton and positron propagation

The exotic antiproton production and propagation have widely been studied in the literature [21, 35, 36, 37, 38], and this also holds for positrons [19, 20, 39, 40]. In this paper, we will use the Green functions as presented in [20] for both the propagations of positrons and antiprotons. Both species experience the same diffusion processes, but have quite different propagation behaviors: positron propagation is mainly affected by Inverse Compton (IC) energy losses, while antiprotons, though their energy losses are negligible, are swept out of the galactic disc (destroyed) by the convective wind (spallations off the interstellar gas) at low energy. Therefore, their respective horizon is completely reversed one from the other in terms of the energy dependence.

The typical propagation length for positrons is given by [19]:

$$\lambda_D = \left\{ \frac{4K_0\tau_E}{1-\delta} (\epsilon^{\delta-1} - \epsilon_S^{\delta-1}) \right\}^{1/2}, \quad (5)$$

where  $\tau_E \simeq 10^{16}\text{s}$  is the characteristic timescale of the energy loss in the IC regime,  $\epsilon \equiv (E/1\text{GeV})$  stands for

the energy at which the positron is detected at the Earth, while  $\epsilon_S \geq \epsilon$  is the energy at which the positron is injected at the source. Given  $\epsilon_S$ , this is clearly a decreasing function of the energy, which is hardly greater than a few kpc.

For antiproton, convection is the relevant quantity that bounds the propagation length, and the horizon is set by [41]:

$$\Lambda_D = \frac{K(E)}{V_{\text{conv}}}, \quad (6)$$

which is, contrarily to the positron case, an increasing function of the energy, and which can quickly get values much greater than the typical size of the diffusion zone.

The characteristic lengths for both antiprotons and positrons are reported in Fig. 2, as functions of the detected energy at the Earth. For positrons, we have considered different injected energies  $E_S$  of 250, 500 and 1000 GeV, and  $\lambda_D$  is plotted as a function of the fraction of  $E_s$  still carried by the particle at the Earth. For antiprotons, we have plotted  $\Lambda_D$  as a function of the detected energy divided by 1 TeV.

These quantities are very useful to figure out the volume from the Earth we are sensitive to when computing the exotic antimatter fluxes. When the positron (antiproton, respectively) energy is high (low), contributions to the flux are mostly local, and large fluctuations are therefore expected if the Earth position is varied inside an N-body environment because the dark matter density varies. This is the contrary at low (high) energies, for which contributions are integrated inside much larger volumes, and tend to smooth the density gradients.

This will be discussed in more details in Sect. V A 2 and V A 3, but the reader can already look at Fig. 4, where it is shown that different local distributions of dark matter strongly affect the positron and antiproton signals, at high and low energy respectively.



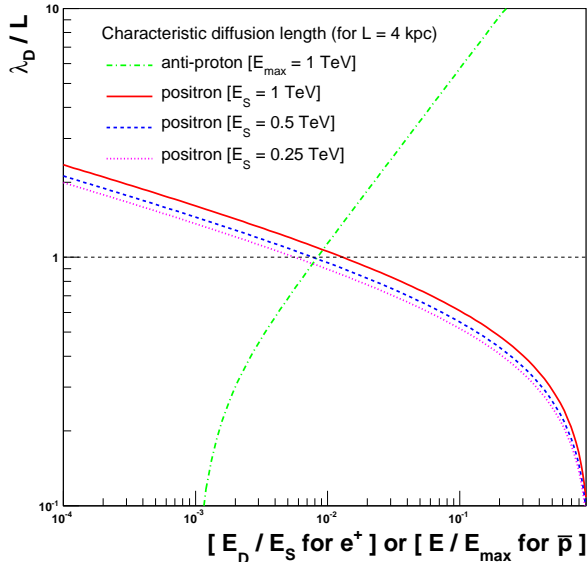


Figure 2: Propagation scales for positrons and antiprotons as functions of energy. For the former, the energy reported on the  $x$  axis is  $E_d/E_s$ , that is the detected energy divided by the injected energy (positrons loose energy), and for the latter, this is merely  $E/E_{\max}$ . Scales are normalized to  $L = 4$  kpc, the vertical half-height of the diffusion zone.

### B. Connection to the N-body source term

N-body simulation results consist in a set of points with coordinates and masses. Though all points correspond to particles of the same mass, the algorithm of density computation defined in Sect. II allows to associate a dark matter density to each point, which actually reflects the particle number density in the point neighborhood. Therefore, each point will be considered as an individual source term of Eq. (3). In order to compute the antimatter flux at the Earth, we have to fix the locations of the Earth and of the diffusion zone with respect to the N-body system of coordinates. Due to the cosmological origin of our simulation, we have no freedom in rescaling the distances, so that the Earth is set at  $R_{\oplus} = R_{\odot} = 8$  kpc, while the Euler angles are random parameters. Once the Earth position is set, we also have to randomly fix the slab diffusion zone, where obviously, the Earth itself is located.

As already detailed in [20], constraints on the local dark matter density are very important for indirect detection of dark matter with antimatter cosmic rays, because local contributions dominate the signal in energy ranges depending on the species (high/low energy for positron/antiproton). Therefore, it is meaningful to add a prescription on top of the random procedure described above, so as to account for the observational constraints on the local dark matter density. According to [20] (and

references therein), it is reasonable to bracket  $\rho_{\odot}$  within  $[0.2, 0.4]$   $\text{GeV} \cdot \text{cm}^{-3}$ . Notice that such a constraint is by itself a very strong limit on the possible variations of the expected fluxes. This will be discussed in Sect. V.

For visual purpose, we show in Fig. 1 projections of the dark matter density  $\rho$  in the diffusion slab according to three different positions for the Earth, at 8 kpc along each axis  $x$ ,  $y$  and  $z$ , respectively (the associated local densities are  $\rho_{\odot} = 0.23, 0.28, 0.13$   $\text{GeV}/\text{cm}^3$ ). These can be seen as different maps of the source term of the diffusion equation (3) (the actual source term is in fact more contrasted because scaling like  $\rho^2$ ). Note that those three different configurations are typified by very different local environments, with sizable density fluctuations, and one can expect some variations on the predicted antimatter cosmic ray fluxes (to go straight to the results, see Fig. 4).

## IV. WIMP MODELS

Despite its numerous successes, the high energy physics standard model of elementary particles needs some extensions. Indeed, some questions like the hierarchy problem, the force unification or the neutrino masses can not be answered without advocating new physics. Furthermore in a large variety of standard model extensions, new particles should be present and some of them could be WIMPs and candidates to dark matter. Some of those scenarios have deep theoretical motivations. Supersymmetric models like the Minimal Supersymmetric Standard Model (MSSM) are inspired from supergravity or string theory and predict new particles below the TeV(s) scale. Those theoretical frameworks also require the existence of extra spatial dimensions, and have inspired the building of phenomenological models in which new particles related to those new dimensions can arise at energies as low as the TeV scale. Some more effective models propose to extend the standard model in more minimal ways, in order to address some specific questions and to consider new phenomenologies without hypotheses on the tricky and unsolved question of the link with some possible fundamental aspects or inspiring sector. After a model independent setting, we will describe some typical benchmark situations of the MSSM, Kaluza-Klein dark matter, Little Higgs Model and Inert Doublet Model, of which we will further survey the signatures in the antimatter cosmic ray spectra.

Note that all cosmic ray spectra for the WIMP models discussed in this paper have been generated with the PYTHIA Monte Carlo [42], and some of the associated relic densities have been computed with the micrOMEGAs code [43].

## A. Model-independent setting

To allow discussion in a very general context, we define here two WIMP fiducial models associated with positron and antiproton production, respectively. For both models, we will take a WIMP mass of 200 GeV and a total annihilation cross section of  $\langle\sigma_{\text{ann}}v\rangle = 3 \times 10^{-26} \text{ cm}^3/\text{s}$ .

The first one, associated with positrons, is either a bosonic or a Dirac fermionic WIMP and is supposed to provide monochromatic electrons and positrons by fully annihilating like  $\chi\bar{\chi} \rightarrow e^+e^-$ . This might, though very roughly, mimic Kaluza-Klein dark matter (see Sect. IV B 2). Such a model greatly simplifies the calculation for the positron flux since the source term is  $\propto \delta(E - m_\chi)$ , and is very convenient to discuss the main features of our results.

The second one, associated with antiprotons, is a Majorana fermionic WIMP that fully annihilates in  $b\bar{b}$ . Such a model is generically found in SUSY theories (see Sect. IV B 1).

## B. Models observable at the LHC

We will show the resulting cosmic ray fluxes from WIMP annihilation in some popular BSM frameworks relevant at the LHC scale that we describe in the next paragraphs.

### 1. The Minimal Supersymmetric Standard Model

The most popular new symmetry of high energy physics is the supersymmetry (SUSY) [44]. The simplest extension in this way is known as the Minimal Supersymmetric Standard Model (MSSM) [45]. The gauge group is still  $SU(3) \times SU(2) \times U(1)$  and the supersymmetric transformations associate a scalar (fermion) to each fermion (boson) of the standard model. This model unifies the coupling constants of the three forces at high energy and nicely achieves the electroweak symmetry breaking through radiative corrections. It requires two Higgs doublets and we note  $\mu$  the mass parameter of those (super)fields and  $\tan\beta$  the ratio of their vacuum expected value (vev). This model has numerous (106) parameters but is usually simplified assuming at high energy unified values for scalar ( $m_0$ ) and fermions ( $m_{1/2}$ ) masses and for trilinear couplings ( $A_0$ ). Thanks to the requirement of radiative electroweak symmetry breaking, the last parameter is the sign of  $\mu$ . The set  $\{m_0, m_{1/2}, \tan\beta, \text{sign}(\mu)\}$  defines a so called Constrained Minimal Supersymmetric Standard Model [46, 47] (CMSSM or mSUGRA) point. In the main part of this parameter space, the dark matter particle is the lightest neutralino,  $\chi_1 \equiv \chi \equiv DM$ . The four neutralinos  $\chi_{1,2,3,4}$  are the mass eigenstates coming from the mixing of neutral Higgs and gauge boson superpartners. There were many studies dedicated to

predictions for antimatter fluxes with SUSY dark matter, see e.g. [21, 39, 48, 49].

Inspired from the SnowMass Point and Slope [50] definition, we will study in the following some typical benchmark points. We have chosen three points as close as possible to SnowMass points but respecting the WMAP constraint. For the sake of completeness, we also relaxed the GUT scale universality assumptions to obtain two additional points providing light neutralinos inspired by [51, 52] and potentially observable at the LHC (see the main parameters in Tab. II).

### 2. Extra dimensions

Initially inspired by the hierarchy problem, large extra dimensions with testable ( $\lesssim \text{TeV}$ ) phenomenological consequences have been studied during the last ten years. For dark matter phenomenology, two kinds of models have been proposed. Either universal large compact extra dimensions with flat geometry [53] where all the Standard Model fields may propagate, or extra dimensions with warped geometry [54, 55] where all fields but the Higgs are in the bulk.

New particles arise as the Kaluza-Klein (KK) modes associated to each standard field.

In universal extra dimensions (UED), the KK parity (coming from translational invariance) implies that the lightest KK particle (LKP) is stable. Consequently, the first mode of neutral particles (mainly photon and Z but also neutrino) can be interesting WIMP candidates. The tree level masses are degenerate and  $= n/R$ , where  $R$  is the size of the compact dimension and  $n$  is the mode number. The radiative corrections add extra terms breaking the degeneracies and in the gauge boson sector, the electroweak symmetry breaking induces mixing between the gauge eigenstates. These contributions lead to different masses for the Z and photons modes. The dark matter particle is most likely a gauge boson. Here, we will consider the LKP dark matter model of [56], which is the first KK excitation of the  $B^{(1)}$  boson. Previous analyses involving this model in the frame of antimatter cosmic rays can be found in e.g. [37, 40, 57].

In warped geometry, one has to impose a  $Z_3$  symmetry to preserve proton stability. Consequently, the lightest  $Z_3$  charged particle (LZP) is also stable and has to be the KK RH neutrino to be a WIMP candidate [58, 59]. The dark matter particle is thus a Dirac fermion. The 4-D masses arise from the localization of wave function of massless modes along the 5<sup>th</sup> dimension. This mechanism is popular to explain the structure of Yukawa couplings. For previous studies of indirect detection involving LZP DM candidates, see e.g. [19, 37, 40, 60].

We have selected one UED model and another one in warped geometry (see Tab. II).

### 3. The Inert Doublet Model

The scalar sector is a key point of numerous high energy physics theories, especially for the standard model and some of its extensions. Up to now, no scalar particle has been discovered and this sector is still unknown. The Inert Doublet Model [61] is a more ad-hoc framework, but quite minimal. It is a two Higgs doublet extension of the standard model with a  $Z_2$  symmetry under which one of the doublet and the fields of the Standard Model are even. The  $Z_2$  symmetry is not broken preserving flavor changing neutral currents and forbidding a vacuum expectation value for the odd doublet. This scalar sector provides three additional odd particles, a neutral ( $H_0 \equiv H \equiv DM$ ), a pseudo ( $A_0$ ) and a charged scalar ( $H_+$ ). In our notation, a point of this model is then defined by the mass of the extra scalar particle masses :  $M_{H_0}, M_{A_0}, M_{H_+}$ , the mass of the standard model Higgs  $m_h$  and two scalar potential parameters related to the odd doublet: a mass dimensional parameter  $\mu_2$  and a coupling  $\lambda_2$  (see [62] for more details concerning the parameterization). The neutral extra scalar particle of the model,  $H_0$ , is a typical candidate of WIMP dark matter with an interesting phenomenology. Inspired from an extended study of the dark matter phenomenology of the Inert Doublet Model [62] we have taken two benchmark points respecting the WMAP constraint (see Tab. II).

### 4. Little Higgs Model

Another possibility to solve the hierarchy problem is to build a model such that the Higgs particle appears

---

as a Nambu-Goldstone boson. In the Little Higgs model with T-parity (see [63, 64, 65] and references therein), a global symmetry  $SU(5)$  with locally gauged subgroup  $[SU(2) \times U(1)]^2$  is spontaneously broken down to  $SO(5)$ . The local subgroup is also broken down to the diagonal subgroup  $SU(2) \times U(1)$ , identified with the SM gauge group. To prevent the contributions from the new heavy gauge bosons associated with the enlarged symmetry to spoil the electroweak precision measurements, a  $Z_2$  symmetry, the T-parity, is introduced [66]. Therefore, the lightest T-odd particle, which happens to be the heavy photon  $A_H$ , is a potential candidate for dark matter [67]. Other T-odd heavy bosons include the heavy gauge bosons  $W_H$  and  $Z_H$  and a scalar triplet Higgs boson  $\Phi$ . The parameters of a point in this model will be given by the value of the vev associated with the symmetry breaking  $f$ , the masses of the heavy T-odd bosons,  $m_{A_H}, m_{W_H}, m_{Z_H}$  and  $m_\Phi$ , and the mass of the Higgs particle  $m_h$ . The annihilation of the heavy photon leads to the production of  $W, Z$  or  $h$ . Points that satisfy the WMAP constraint lie on two branches in the plane  $f - m_h$ . For points on the upper branch (U-branch),  $m_h > 2m_{A_H}$ , while for points on the lower branch (L-branch),  $m_h < 2m_{A_H}$  [68]. Therefore, we have selected one benchmark point on each branch (see Tab. II).

To summarize our benchmarks, we have chosen five supersymmetric points, two models with extra dimension, two Inert Doublet points and two Little Higgs models. Parameters and details can be found in Tab. II.

## V. RESULTS AND DISCUSSION

We have performed different calculations in order to extract the most relevant features in a cosmological N-body framework. We will first discuss the theoretical uncertainties on fluxes that we can infer from an analysis using WIMP fiducial models, combining the N-body data with analytical extrapolations. Afterwards, we will focus on the predictions that we can derive out of an averaged description of our 3D dark matter density map for different BSM dark matter particle candidates.

### A. Effects of the dark matter distribution and inhomogeneities

#### 1. Modifications of the spherical smooth profile

Contrarily to dark matter contributions to the Galactic gamma-ray flux, it has long been shown that changes in the inner and outer logarithmic slopes of the smooth dark matter density profile have no significant effects on the charged cosmic ray signatures. This is due to diffusion, which tends to dilute the signal when integrated over large volumes (low/high energies for positrons/antiprotons). This has been checked for this N-body simulation, for which different fits of the density profile give roughly the same statistical description of the data. This is illustrated in Fig. 3, where we plot the positron and antiproton fluxes corresponding to three different fitted profiles, and where we also plot the result obtained with the common NFW model very often used in the literature to describe our Galaxy. The former three are characterized by an averaged density of  $\rho_\odot = 0.25 \text{ GeV/cm}^3$  at 8 kpc from the GC, while the latter is taken with its standard value of  $\rho_\odot = 0.3 \text{ GeV/cm}^3$ . It is noteworthy that there is absolutely no observable difference in the computed fluxes between the former three, and that the latter only gives a very small additional contribution at high (low) energy for positrons (antiprotons). This is merely due to the increase in the local density that translates to a factor of  $(0.3/0.25)^2$  to fluxes for small propagation lengths. This clearly demonstrates that even significant modifications in smooth profiles lead to minor effects, provided the local environment is not too much affected.

#### 2. Departure from spherical symmetry

In the previous paragraph, we have shown that the flux predictions were not sensitive to modifications of smooth spherical profiles. However, it turns out that though dark matter halos are found to be roughly spherically symmetric in N-body simulations in average, they usually do not exhibit such a symmetry when 3-D scrutinized. Furthermore, both observations and dynamical studies support axisymmetry instead [69, 70, 71]. The

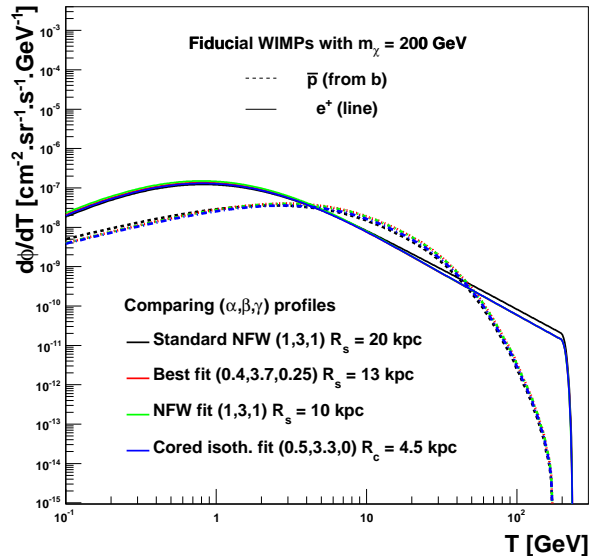


Figure 3: Comparison of positron and antiproton fluxes obtained with different smooth profiles: three are fitted on the HORIZON simulation (best fit, NFW and cored) and the fourth is the standard NFW fit very often used for the Milky Way.

N-body framework allows to directly take the effects of departure from spherical symmetry into account. This may be seen in the left panel of Fig. 4, where we computed the positron and antiproton contributions associated with the three projected density maps of Fig. 1 (an elliptic distortion appears in the  $xy$  plane, along the  $y$  axis). We see that for positrons (antiprotons respectively) the low (high) energy parts of the spectra are superimposed, whereas the high (low) energy parts differ significantly. This comes from that low (high) energy contributions correspond to a signal averaged over large volumes, erasing information on the source geometry. Conversely, local variations of the dark matter density are only relevant at high (low) energies for positrons (antiprotons). Therefore, global geometry modifications such as departure from sphericity can have an important impact if the averaged local dark matter density is changed accordingly. This can be further checked by analytically deforming a spherical halo to model an elliptical one. The recipe is presented in [72], where an elliptical profile of eccentricity  $a$  along the  $x$  axis in the  $xy$  plane can be inferred from the spherical dark matter density according to  $\rho_{\text{elliptical}}(x, y, z) \equiv \rho_{\text{spherical}}(x/a, ay, z)$ . Of course, elliptically modifying the halo shape modifies the local dark matter density in the same time. Fixing the Earth position at  $x = 8 \text{ kpc}$ , we have considered two cases:  $a = 2$  and  $a = 1/2$ , which results in a modification of the local density by a factor of 3.26 and 0.26 respectively. Such modifications are expected to magnify the



Benchmark point	$M_\chi$ (GeV)	$\Omega h^2$	$\langle\sigma v\rangle(\text{cm}^3\text{s}^{-1})$	Branching ratios
SUSY light-1 : light neutralino, annihilation through $A$ funnel (scenario A [52] like) Non universal parameters	9.7	0.116	$2.17 \times 10^{-26}$	$BR(\chi\chi \rightarrow b\bar{b}) = 0.873$ $BR(\chi\chi \rightarrow \tau^+\tau^-) = 0.125$
SUSY light-2 : light neutralino, annihilation into $\tau^+\tau^-$ via $\tilde{\tau}$ (scenario B [52] like) Non universal parameters	34.1	0.129	$1.48 \times 10^{-26}$	$BR(\chi\chi \rightarrow \tau^+\tau^-) = 1$
SUSY-SPS2 : focus point, mixed higgsino-gaugino neutralino (SPS2-like) $m_0=2850$ GeV, $m_{1/2}=500$ GeV, $A_0=0$ GeV, $\tan\beta=10$ $\mu>0$	198.7	0.102	$2.30 \times 10^{-26}$	$BR(\chi\chi \rightarrow t\bar{t}) = 0.719$ $BR(\chi\chi \rightarrow ZZ) = 0.0763$ $BR(\chi\chi \rightarrow s\bar{s}) = 0.00387$
SUSY-SPS3 : neutralino-stau coannihilation (SPS3-like) $m_0=150$ GeV, $m_{1/2}=680$ GeV, $A_0=0$ GeV, $\tan\beta=10$ $\mu>0$	283.8	0.102	$2.08 \times 10^{-29}$	$BR(\chi\chi \rightarrow b\bar{b}) = 0.733$ $BR(\chi\chi \rightarrow \tau^+\tau^-) = 0.176$ $BR(\chi\chi \rightarrow t\bar{t}) = 0.0762$
SUSY-SPS4 : bino neutralino with main annihilation through Higgs funnel (SPS4-like) $m_0=770$ GeV, $m_{1/2}=600$ GeV, $A_0=0$ GeV, $\tan\beta=50$ $\mu>0$	252.2	0.107	$1.50 \times 10^{-26}$	$BR(\chi\chi \rightarrow b\bar{b}) = 0.849$ $BR(\chi\chi \rightarrow \tau^+\tau^-) = 0.147$ $BR(\chi\chi \rightarrow s\bar{s}) = 0.00387$
KK-1 : KK right-handed neutrino (warped-GUT-like). KK boson mass scale $M_{KK} = 6$ TeV	50	$\simeq 0.1$	$2.04 \times 10^{-26}$	$BR(\chi\chi \rightarrow b\bar{b}) = 0.7$ $BR(\chi\chi \rightarrow l^+l^-) = 0.035 \times 3$ $BR(\chi\chi \rightarrow \nu\bar{\nu}) = 0.065 \times 3$
KK-2 : first excitation of the $B^{(1)}$ gauge boson (UED-like)	1000	$\simeq 0.1$	$1.7 \times 10^{-26}$	$BR(\chi\chi \rightarrow l^+l^-) = 0.19 \times 3$ $BR(\chi\chi \rightarrow (q\bar{q})_u) = 0.1 \times 3$ $BR(\chi\chi \rightarrow \nu\bar{\nu}) = 0.04 \times 3$ $BR(\chi\chi \rightarrow (q\bar{q})_d) \simeq 0.01 \times 3$
IDM-1 : light dark matter, annihilation through $A$ funnel $\mu_2=35$ GeV, $\Delta M_{A_0}=10$ GeV, $\Delta M_{H^+}=50$ GeV, $m_h=120$ GeV, $\lambda_2=0.1$	45	0.109	$1.23 \times 10^{-27}$	$BR(\chi\chi \rightarrow b\bar{b}) = 0.871$ $BR(\chi\chi \rightarrow \tau^+\tau^-) = 0.0435$ $BR(HH \rightarrow c\bar{c}) = 0.0835$
IDM-2 : heavy dark matter, annihilation into gauge bosons $\mu_2=1005$ GeV, $\Delta M_{A_0}=5$ GeV, $\Delta M_{H^+}=10$ GeV, $m_h=120$ GeV, $\lambda_2=0.1$	1000	0.117	$4.04 \times 10^{-26}$	$BR(HH \rightarrow W^+W^-) = 0.589$ $BR(HH \rightarrow ZZ) = 0.223$ $BR(HH \rightarrow hh) = 0.174$
LHM-1 : L-branch $f=702$ GeV, $m_{A_H}=103$ GeV, $m_{W_H}=450$ GeV, $m_{Z_H}=450$ GeV, $m_\Phi=484$ GeV, $m_h=120$ GeV	103	$\sim 0.13$	$1.4478 \times 10^{-26}$	$BR(HH \rightarrow W^+W^-) = 0.7343$ $BR(\chi\chi \rightarrow ZZ) = 0.2657$
LHM-2 : U-branch $f=1050$ GeV, $m_{A_H}=162$ GeV, $m_{W_H}=678$ GeV, $m_{Z_H}=678$ GeV, $m_\Phi=2410$ GeV, $m_h=400$ GeV	162	$\sim 0.13$	$1.9 \times 10^{-26}$	$BR(\chi\chi \rightarrow W^+W^-) = 0.6893$ $BR(\chi\chi \rightarrow ZZ) = 0.3107$

Table II: Benchmark points used in the calculation for Fig 7.

differences in fluxes observed in the left panel of Fig. 4. The full calculation indeed leads to the right panel of Fig. 4, where the former (latter) case is clearly shown to enhance (decrease respectively) the positron and antiproton fluxes by 1 order of magnitude, but mainly at energies corresponding to short propagation lengths. The effect is much less important at energies corresponding to large propagation lengths, where the spherical halo predictions are asymptotically recovered. The two previous examples are extreme configurations compared to the current observational constraints, and are likely to be attenuated by the measured angle of  $\phi \sim 20^\circ$  between the GC - Earth axis and the semi-major axis [69].

### 3. Density fluctuations and sub-halos

Beside global geometry considerations, dark matter inhomogeneities are expected to play a much more important role in characterizing the dark matter contribution to the antimatter spectra, but mostly at energies corresponding to small propagation scales. Indeed, at energies for which the propagation scale is large, the argument is the same as previously, and diffusion erases the effect of the source term fluctuations (contributions from the Galactic center dominate). On the contrary, the asymptotic limit of fluxes for energies  $\tilde{E}$  corresponding to very short propagation scales only depends on the local dark matter density. As already stressed before, the main interest of using an N-body framework is to access a realistic inhomogeneous distribution of dark matter. By setting the terrestrial observer at different places in the N-body galaxy, we can survey the effect of density spatial fluctuations, that is the effect of modifying the local environment. This is illustrated in Fig. 5, where we plot the flux predictions for positrons (left panel) and antiprotons (right panel) associated with 100 different positions of the Earth within our N-body grid (the galactocentric radius is fixed at 8 kpc). For comparison, we report on the same figures the results when using the best-fit smooth profile, as well as the existing data (from [73, 74, 75] for positrons, and from [75, 76, 77, 78, 79] for antiprotons). What is interesting is, again, that contributions at energies corresponding to large propagation scales (high/low for antiprotons/positrons) are very well featured by a smooth description, while fluxes corresponding to small propagation scales fluctuate a lot. Such fluctuations are due to modifications of the local dark matter density. The larger fluctuations come from configurations for which the local density is not constrained to be within  $[0.2, 0.4] \text{ GeV.cm}^{-3}$  (green curves – the black ones are density-constrained). It is easy to quantify the amplitudes of these fluctuations, since the asymptotic flux (small propagation scales) merely scales like  $\rho_\odot^2$ . The value of  $\rho_\odot = 0.25 \text{ GeV.cm}^{-3}$  used for the smooth profile allows to have an idea of the local dark matter densities corresponding to the extremal fluxes showed in Fig. 5, which spread over two orders of magnitude (a factor of

$\sim 2$  for maximal, and a factor of  $\sim 1/4$  for minimal local densities).

Although we can nicely deal with density fluctuations in our N-body galaxy, the lack of resolution at small scales prevent us to resolve sub-halos less massive than  $\sim 10^7 M_\odot$ . Moreover, more massive sub-halos are only found at the periphery of our simulation data, well beyond the cosmic ray diffusion zone, and we do not have evidence for other sub-halos in the solar neighborhood that could affect the antimatter flux predictions. Sub-halos are expected to have much more important impacts on predictions because they are not merely density fluctuations: they are structured objects with inner profiles, the first virialized objects of the universe, of which the central density could be as or even more cuspy than the galactic center itself. The source term of antimatter production scaling like the squared density, sub-halos are therefore likely to constitute a major component of the exotic primary fluxes. Of course, some better simulations have already achieved resolutions good enough to resolve clumps as light as  $\sim 10^5 M_\odot$  (e.g. the Via Lactea simulation described in [24]), but they are still very far from the typical minimal masses  $\sim 10^{-6} M_\odot$  set by the free streaming scales inferred from particle physics. Consequently, the intrinsic resolution limits of simulations make the use of analytical extrapolations unavoidable in order to study the effects of the smallest dark matter structures on predictions. Besides and fortunately, the case of antimatter cosmic rays is well suited for such approaches, because contrarily to gamma-rays, the precise location and internal features of any source are by no means observable with such messengers. Furthermore, an analytical and statistical recipe for calculating any clump configuration contribution to the antimatter primaries has been very well defined and described in [19] and [20]. The latter reference provides an exhaustive and detailed method to deal with sub-halos as characterized in  $\Lambda$ -CDM cosmology. Armed with these analytical device, we can extrapolate our results to different sub-halo configurations, all typified by a  $M^{-\alpha_M}$  mass distribution, inner profiles and concentrations, and eventually by a spatial distribution.

We have considered two specific cases. The first one is an optimistic *maximal* case in which clumps are as light as  $10^{-6} M_\odot$ , with  $\alpha_M = 2$ , inner NFW profiles, and obey the so-called Bullock – B01 – concentration-mass relation [80]; in this configuration, we make sub-halos spatially track the smooth profile. The second one is approximately reminiscent from what the authors of [24] found in their Via Lactea simulation, and will be referred to as the *Via-Lactea-like* configuration. It is featured by a minimal clump mass of  $10^6 M_\odot$ ,  $\alpha_M = 1.9$  – i.e.  $\sim 10^{12}$  times less clumps than in the *maximal* case –, inner NFW profiles, B01 concentrations, and a spatial distribution antibiased with respect to the smooth profile (see [81] for more details on the *spatial antibias*). The reader is referred to [20] for more insights on the impact of the clump parameters on predictions for the antimatter cosmic ray fluxes. We plot the positron and antiproton fluxes for

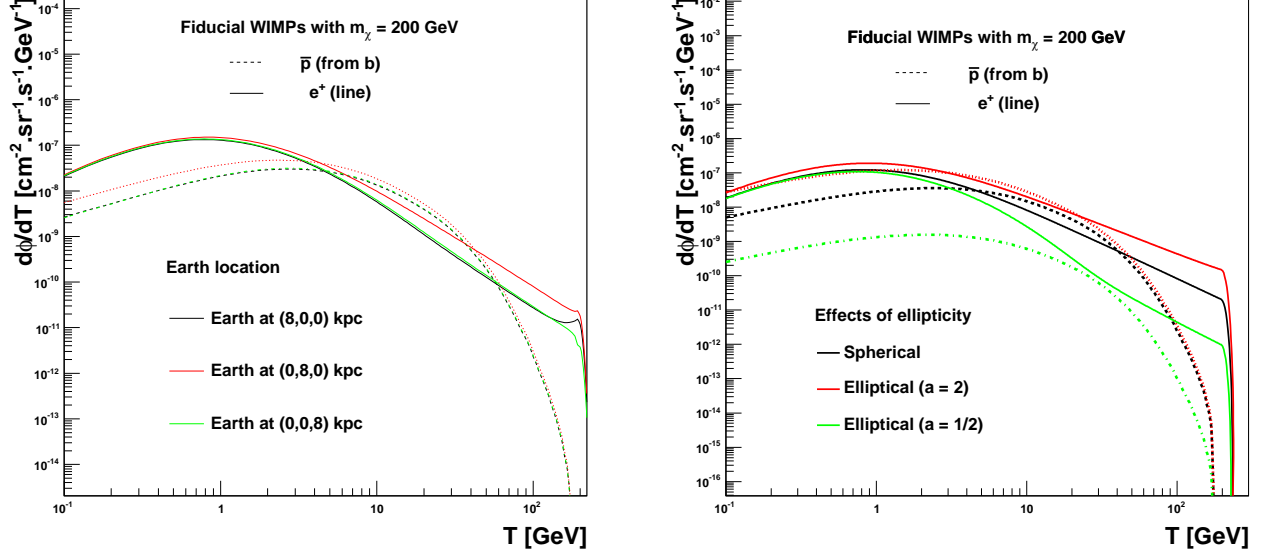


Figure 4: Positron and antiproton fluxes. Left panel: those corresponding to the three different Earth positions illustrated in Fig. 1. Right panel: taking into account an elliptical deformation of the dark matter halo (see the details in Sect. V A 2. All fluxes are computed with the fiducial WIMP models (see Sect. IV A).

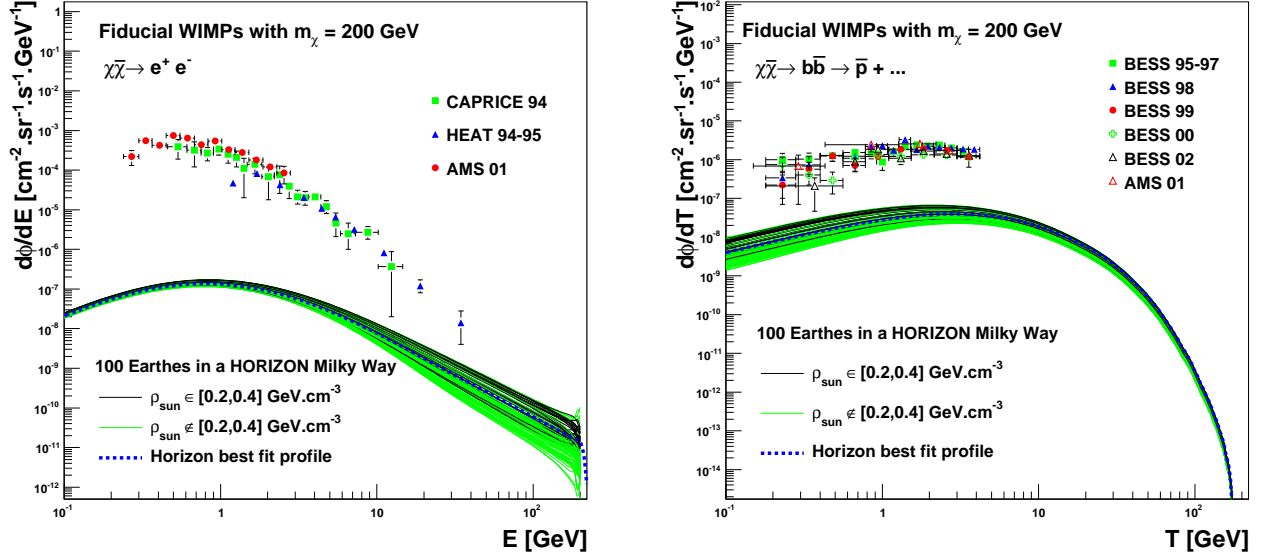


Figure 5: Varying the Earth position in the N-body simulation. 100 random positions are sorted and fluxes are computed for positrons (left) and antiprotons (right). Fiducial WIMP models detailed in Sect. IV A are used.

both configurations in Fig. 6, which somehow quantifies the consequences of our lack of spatial resolution, and might even allow to by-pass it. These fluxes are characterized by mean values and associated statistical variances (shown as contours) taking into account probabilities for clumps to be located inside the relevant (energy

dependent) diffusion volume and to contribute to the signals; in both configurations, the smooth halo is described by our best fit parameters (see Sect. II). The *maximal* configuration (left panel) unveils a flux enhancement (so-called *boost factor*) with respect to the contribution of the smooth dark matter component which depends on the

energy, and saturates at energies corresponding to small propagation scales. Indeed, the smooth central halo contribution strongly dominates the signals against clumps at large propagation scales, whereas clumps are likely to overcome at small propagation scales if numerous enough in the local environment [19, 20]. The maximal boost factor is  $\sim 4$ , which gives an idea of what we could expect from such a small scale clumpiness. Taking a  $r^{-1.5}$  profile inside clumps instead of NFW would provide an additional factor of  $\sim 10$ . The *Via-Lactea-like* configuration does not provide any flux enhancement in average, but the statistical variance of signals is still relevant at short propagation scales, for which a very close object, a very improbable situation, could increase the signals. Notice that the sub-halo effects yield uncertainties of the same order of magnitude as the density fluctuations and departure from spherical symmetry previously considered.

### B. Predictions for different dark matter particle candidates

After having tried to quantify the effects coming from possible dark matter density fluctuations with a WIMP model-independent setting, it is useful to restore those predictions in a more constrained particle physics scheme. This really allows to define and compare the flux orders of magnitude that WIMP searches do have to deal with. To this aim, we have used an Earth location in the N-body frame which provides intermediate fluxes as illustrated in Fig. 5, with a local density of  $\rho_\odot \simeq 0.25 \text{ GeV.cm}^{-3}$ .

We have derived predictions for all dark matter candidates presented in Sect. IV, of which the features are summarized in Tab. II – some of them are detectable at the LHC, with well defined related signatures. The positron (left) and antiproton (right) fluxes are reported in Fig. 7 for SUSY (top) and non-SUSY particles (bottom panels, respectively). On the same panels are pictured the existing data (from [73, 74, 75] for positrons, and from [75, 76, 77, 78, 79] for antiprotons). From this figure, we clearly see that only the lightest SUSY candidate is about to imprint the antiproton spectrum, but at very low energies ( $\lesssim 1 \text{ GeV}$ ), a spectral region which very much suffers from solar modulation effects (the scatter in the low energy BESS data points is mainly due to different solar activities during the observations). All other candidates remain far lower than the existing data, and are therefore poorly constrained. Even a one order of magnitude enhancement, due to the various effects considered above, would not be enough to detect nor constrain the studied dark matter candidates with the current data.

The previous statements rely of course on the fact that the propagation model we used is defined by the median set of propagation parameters of Tab. I. A more favorable set, which for instance would involve a larger diffusion coefficient  $K$  and a larger vertical extension

$L$  of the diffusion zone (such that  $K/L$ , the main constrained quantity, remains constant), could lead up to an additional order of magnitude in terms of fluxes (see e.g. [20, 21, 23]), and could therefore make of the current data very strong limits. This points towards the necessity to have more precise and over larger energy ranges data of secondary/primary cosmic rays to much better bound the propagation allowed configurations. Furthermore, we see on Fig. 7 that there is an overwhelming lack of high energy data above  $\sim 10 \text{ GeV}$ , precisely in spectral regions where the astrophysical background coming from secondaries is expected to be power law suppressed. Higher energy data could indeed exhibit a spectral transition due to an exotic component, provided the dark matter candidate is massive enough. The PAMELA satellite is currently improving the measurements on antiprotons and positrons in a slightly higher energy range than before [82], and the GLAST satellite will also have the potential to detect high energy electrons and positrons [83].

### C. Limits of the N-body framework

N-body simulations are the only way to scrutinize structures that have virialized in the non linear regime, and especially when one is interested to check some peculiar effects, such as those coming from inhomogeneities or asphericity. Nevertheless, such a framework still suffers from many drawbacks, due to their incompleteness. First of all, the limited spatial resolution prevents the study of the smallest scales that substructures can have, and which are fixed by the free streaming length of dark matter particles in the early universe. Some authors have tried to tackle this issue, by performing simulations resolving  $\sim 10^{-6} M_\odot$  objects, but their results hold only at a redshift  $z = 26$ , when galactic halos are not yet formed [84]. Even by taking the fastest available supercomputers for cosmological simulations, the authors of [24] only reached a resolution allowing the identification of  $\sim 10^5 M_\odot$  objects, that is more than 10 orders of magnitude beyond what is expected from WIMP cold dark matter.

Moreover, it is noteworthy to recall that baryons are likely to play an important role in the dynamics of galaxies, and they are not yet fully incorporated in cosmological simulations down to the galactic scale. For instance, galactic bars observed in the centers of spirals have long been shown to exchange momentum with the dark matter halo, and are therefore expected to modify the dark matter distribution (see e.g. a recent analysis in [71], and references therein). Moreover, it is well known, but scarcely mentioned in the present context, that the available data on the dynamics of the Milky Way, the target of interest in this paper, strongly disfavor cuspy halo models (see more general arguments in e.g. [85]).

In order to illustrate this statement, we have used the kinematic data provided by [86], for which the authors subtracted the contribution from the baryons as de-



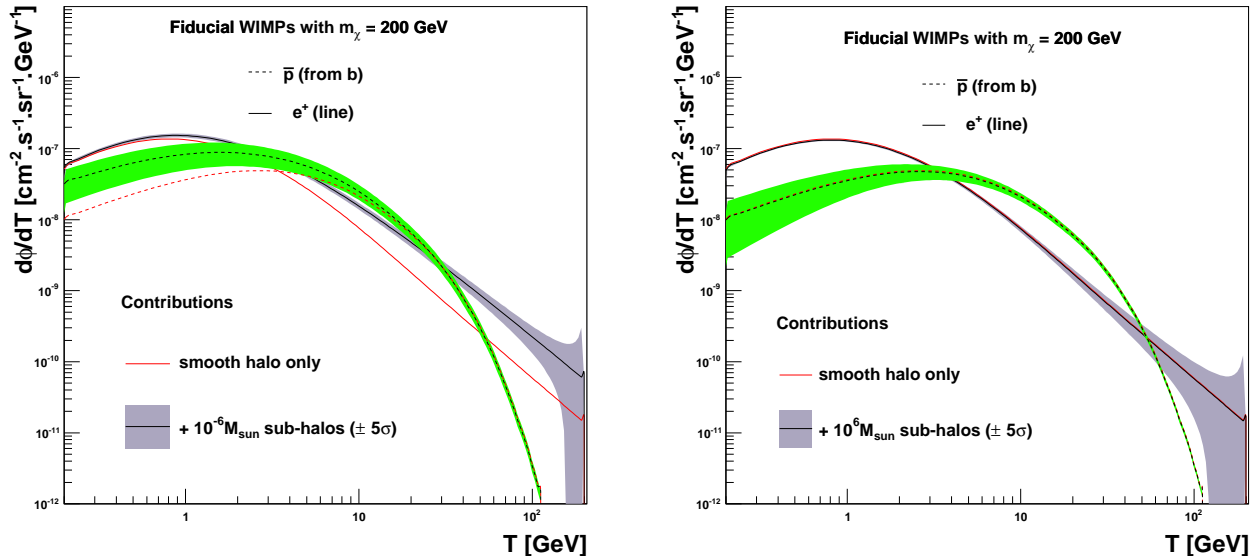


Figure 6: Analytical predictions for the positron and antiproton fluxes when considering sub-halos in the Horizon framework. Left panel: *maximal* configuration, where  $10^{-6} M_{\odot}$  NFW clumps are involved. Right panel: *Via-Lactea-like* configuration, where we consider  $10^6 M_{\odot}$  NFW sub-halos. Fiducial WIMP models detailed in Sect. IV A are used.

scribed by the bulge-disc-bar model of [70]. In Fig. 8 (left panel), we have reported the circular velocities against the galactocentric radius, inferred from the smooth dark matter profiles fitted on our N-body data and presented in Sect. II, from the standard NFW profile, and also from a toy model with parameters  $\alpha = 2$ ,  $\beta = 1$ ,  $\gamma = 0.5$ ,  $r_s = 10$  kpc,  $\rho_{\odot} = 0.5 \text{ GeV.cm}^{-3}$  (cf. Eq. 2). The latter has no physical justification at all, and has only been tuned to correctly adjust the velocity data. For comparison, we have plotted the same profiles against the density data extracted from our N-body simulation (right panel).

Disregarding the toy model for the moment, it is interesting to realize that while the standard NFW hardly better fits the velocity curves than the others at large radii ( $r \gtrsim 6$  kpc), all the cuspy profiles fail to reproduce the dark matter rotation curve in the inner 4 kpc. They lead to an overestimate of the dark matter mass. Between 4 and 8 kpc the fits are also bad, but take advantage of the large dispersion of the observational points to remain within the cloud of points. However, they adjust the highest values at the inner radii and the lowest values at the largest radii, i.e. are not acceptable in the  $\chi^2$  squared sense. Beyond 8 kpc the values predicted by the cuspy profiles are by far too low compared to the observations, even when one takes into account the considerable uncertainties of the observations outside the solar radius. The toy model, which is close to a cored isothermal profile, provides a good fit to the observations, which is not surprising since it was tuned for this purpose, but, interestingly, does not fit the N-body data. This underlines one of the well known and much discussed discrepancies

between observations and the cosmological N-body simulations in the scale of galaxies. Such discrepancies are believed to be due to the fact that cosmological N-body simulations do not include yet the baryonic component, of which the presence could lower the cusp into a core.

Hence, we stress that the predictions we provided in the previous section should be better considered as indicative, because they do certainly not contain the full theoretical uncertainties, especially those coming from our ignorance of the baryon influence. Nevertheless, such a treatment in an N-body context still allows a better understanding of the uncertainties which come from the possible fluctuations of our local dark environment. Computing the fluxes by using the previously discussed toy model profile would give exactly the same trend as those reported in Fig. 3, with a slightly increased asymptotic value at short cosmic ray propagation scales, by a factor of  $(\rho_0^{\text{toy}}/\rho_0^{\text{horizon}})^2 = 4$ . In order to not further complexify the reading, we do not plot the corresponding predictions, since this toy model does not rely on any theoretical motivation. Eventually, despite the cited drawbacks, such an analysis sketches the bases for further studies using more complicated frameworks (including baryons for instance).

## VI. CONCLUSION

In this paper, we have studied the theoretical uncertainties associated with dark matter density fluctuations affecting the primary antimatter cosmic ray fluxes

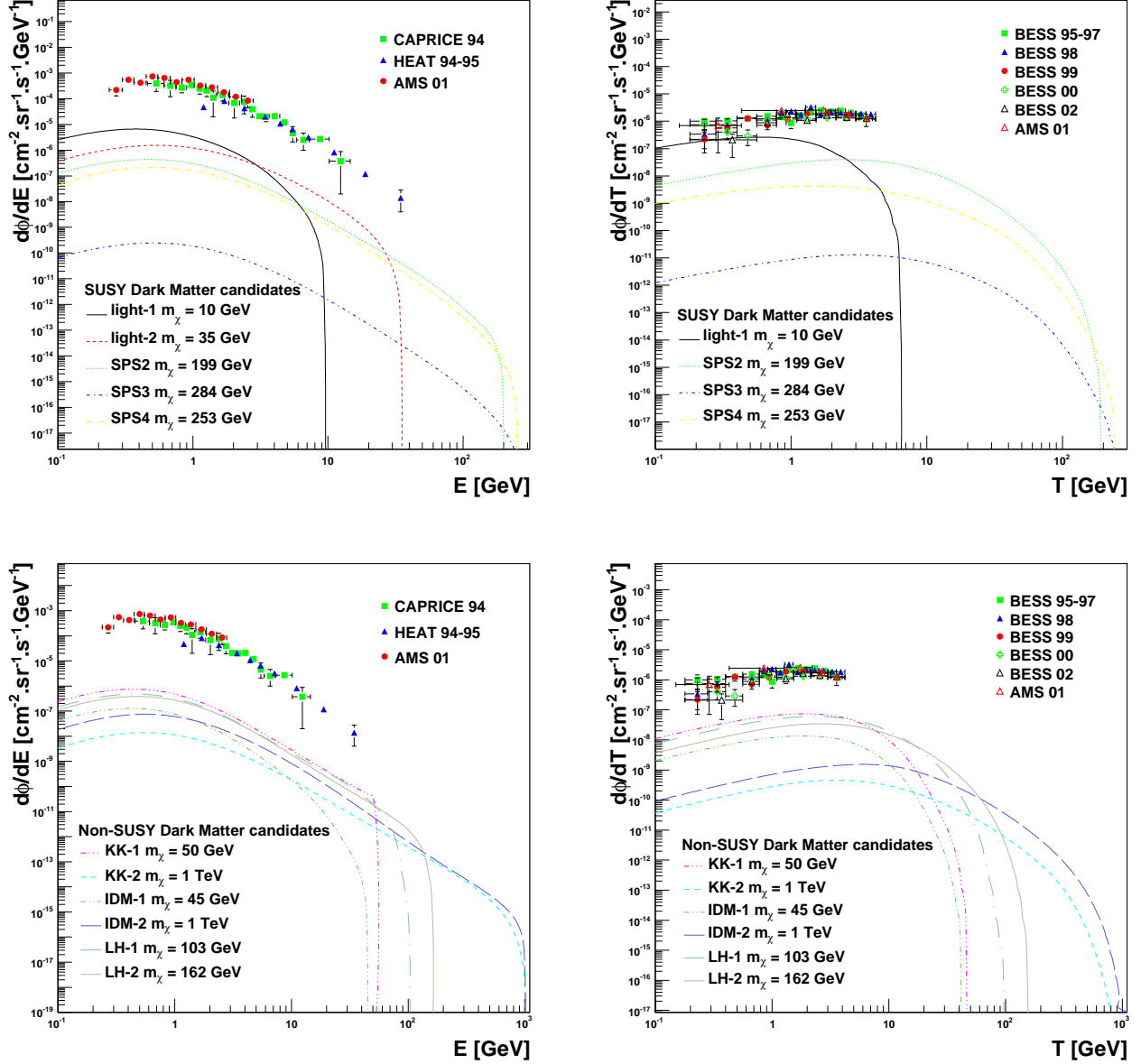


Figure 7: Left: positron fluxes for SUSY dark matter (top) and non-SUSY dark matter (bottom). Right: same as left panels but for antiprotons.

(positrons and antiprotons), possibly produced by dark matter annihilation in the Galaxy, by using an N-body simulation together with analytical descriptions of a galaxy-like dark matter halo. This is the first attempt in this research field to directly connect the source term of the cosmic ray propagation equation to a 3D density map coming from a cosmological N-body framework, while this has already often been used for predictions of gamma-ray fluxes. Indeed, the latter situation does not involve cosmic ray propagation, which seriously complicates the calculations, and makes them much more time consuming. The main purposes of this work was to

quantify those uncertainties, and in some cases to try to understand them by analytical means. While this was achieved in a WIMP model-independent setting, we also aimed at reviewing the status of predictions for many different well motivated dark matter candidates in particle physics, supersymmetric or not.

The N-body framework led us to study several effects, such as non-spherical dark matter distributions (Sect. VA 2) and density fluctuations (Sect. VA 3), which are not accounted for when using the traditional spherical smooth halo models. We have shown that, as expected, fluxes are mainly affected at cosmic ray en-

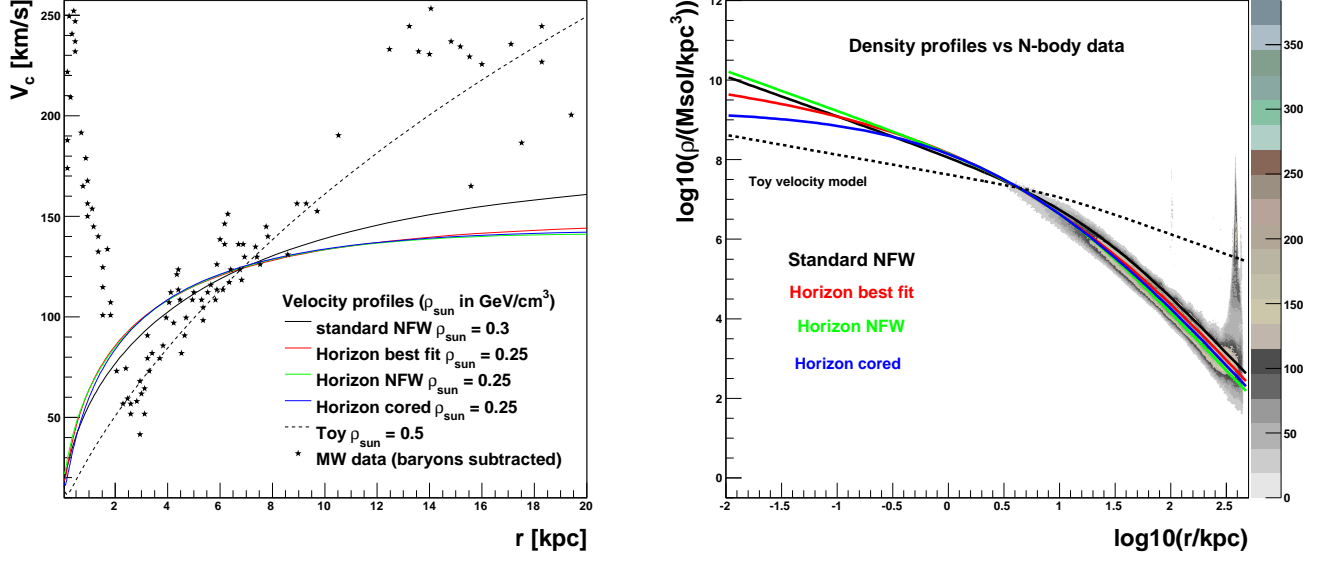


Figure 8: Left: Radial velocities inferred from the spherical dark matter halo models discussed in Sect. II, plus a toy model with  $\alpha = 2$ ,  $\beta = 1$ ,  $\gamma = 0.5$ ,  $r_s = 10$  kpc,  $\rho_\odot = 0.5 \text{ GeV.cm}^{-3}$ . The stars represent the kinematic data from which the baryonic contribution has been subtracted ; cf. Fig. 3 of [86]. Right: same density profiles reported on the N-body density data, for comparison.

ergies corresponding to short propagation characteristic lengths (low/high for antiprotons/positrons) and to local contributions, while when looking at energies of large propagation lengths, the smoothing due to diffusion erases the peculiarities in the spectra, and is well reproduced by a spherical halo model. The main uncertainties on the predicted fluxes come therefore from those on the local dark matter environment, which we have shown to fluctuate a lot in the N-body framework. This can lead to  $\pm 1$  order of magnitude in terms of flux, at high energy for positrons, and low energy for antiprotons. This could be more constrained with much better limits on the local dark matter density.

Moreover, though our simulation has a too poor spatial resolution to resolve substructures inside the galactic halo, we have extrapolated our results in order to include the potential effects of the presence of sub-halos by using the analytical method detailed in [20]. We have considered two situations: one *maximal*, analytically extending the clump mass spectrum down to  $10^{-6} M_\odot$ , led to a flux enhancement by an energy-dependent factor reaching  $\sim 4$  at maximum; a second, *Via-Lactea-like*, involved clumps down to  $10^6 M_\odot$  only and did not result in any flux enhancement.

Consequently to the previous points, the smooth and spherical modeling of the dark matter halo leads to a very good approximation of a more complete and complex situation, as derived from an N-body simulation, at large characteristic propagation lengths for antimatter cosmic rays (low/high energies for positrons/antiprotons). Nev-

ertheless, though predictions in the spectral regions associated with those large characteristic scales are also the less affected by the uncertainties coming from dark matter density fluctuations, we remind that they are still very sensitive to the used propagation model.

Beside this trial for directly *measuring* the theoretical uncertainties with an N-body experiment, we reviewed the predictions of the positron and antiproton primary contribution associated with some specific particle physics dark matter candidates (Sect. VB). We have not only included some popular supersymmetric and extra-dimensional models, but also some more specific ones based on minimality arguments, such as the little Higgs model, or the inert doublet model. We have shown that predictions are well lower than the existing data, except perhaps for the antiproton flux associated with the lightest neutralino model, just because of the more favorable  $1/m_\chi^2$  factor appearing in the flux expression. Nevertheless, even if the latter appears in tension with the current data, its contribution to the antiproton flux occurs at energies where solar modulation effects are expected to be important, and it would be hard to find a clear signature in this spectral region. The other models are well below the experimental measures, but higher energy measurements could perhaps unveil some spectral transitions followed by an energy cut-off which could possibly be attributed to dark matter. In this case, uncertainties associated with the dark matter density fluctuations would be much less stringent for the antiproton signal than for the positron because of propagation scale argu-

ments. On the contrary, a nearby clump would favor a detection with positrons at high energy, much more than with antiprotons. Anyway, higher energy data are necessary in this field, for these antimatter species as well as for standard nuclei species which will yield much better constraints to the propagation modeling. Obviously, indications of a WIMP candidate mass, as expected from the LHC, would provide the relevant spectral region where to concentrate the astrophysical searches, and would allow to concentrate on much more subtle effects.

Finally, we made a self-criticism exercise – Sect. V C – by comparing our different halo models to the star kinematic data available for our Milky-Way Galaxy, after subtraction of the baryonic contribution as modeled by [86]. We show that the dark matter contribution to the velocity field as inferred from our N-body simulation, as well as more general ones, are far to reproduce the kinematic data, systematically leading to a mass excess in the central regions ( $\lesssim 4$  kpc) of the Galaxy. This clearly calls

for restraint in our potential claims, and clearly points towards some large amount of ignorance in the intimate (and gravitational) relations between dark matter and baryons.

### Acknowledgement

We would like to thank A. Bosma, N. Fornengo and P. Salati for interesting discussions during this study. This work took advantage of the favorable environment encountered during some of the French GDR SUSY meetings; we are grateful to its current headmaster J. Orloff and to its Dark Matter subgroup coordinators C. Goy and G. Moulhaka for having supported this collaboration. F.-S. Ling has funding from the Belgian FNRS. This work was partly supported by grant ANR-06-BLAN-0172.

- 
- [1] H. Murayama (2007), arXiv:0704.2276.
  - [2] J. R. Primack, Nuclear Physics B Proceedings Supplements **173**, 1 (2007), arXiv:astro-ph/0609541.
  - [3] G. Jungman, M. Kamionkowski, and K. Griest, Phys. Rept. **267**, 195 (1996), arXiv:hep-ph/9506380.
  - [4] L. Bergström, Reports of Progress in Physics **63**, 793 (2000), arXiv:hep-ph/0002126.
  - [5] G. Bertone, D. Hooper, and J. Silk, Phys. Rept. **405**, 279 (2005), arXiv:hep-ph/0404175.
  - [6] J. Carr, G. Lamanna, and J. Lavalle, Reports of Progress in Physics **69**, 2475 (2006).
  - [7] Y. Mambrini, C. Muñoz, and E. Nezri, Journal of Cosmology and Astro-Particle Physics **12**, 3 (2006), arXiv:hep-ph/0607266.
  - [8] J. E. Gunn, B. W. Lee, I. Lerche, D. N. Schramm, and G. Steigman, Astrophys. J. **223**, 1015 (1978).
  - [9] J. Silk and M. Srednicki, Physical Review Letters **53**, 624 (1984).
  - [10] F. Stoehr, S. D. M. White, V. Springel, G. Tormen, and N. Yoshida, Mon. Not. R. Astron. Soc. **345**, 1313 (2003), arXiv:astro-ph/0307026.
  - [11] J. Diemand, M. Kuhlen, and P. Madau, Astrophys. J. **657**, 262 (2007).
  - [12] E. Athanassoula, F. . Ling, E. Nezri, and R. Teyssier, ArXiv e-prints **801** (2008), 0801.4673.
  - [13] M. Kuhlen, J. Diemand, and P. Madau, ArXiv e-prints **805** (2008), 0805.4416.
  - [14] L. Bergström, J. Edsjö, P. Gondolo, and P. Ullio, Phys. Rev. D **59**, 043506 (1999), arXiv:astro-ph/9806072.
  - [15] P. Ullio, L. Bergström, J. Edsjö, and C. Lacey, Phys. Rev. D **66**, 123502 (2002), arXiv:astro-ph/0207125.
  - [16] V. Berezhinsky, V. Dokuchaev, and Y. Eroshenko, Phys. Rev. D **68**, 103003 (2003), arXiv:astro-ph/0301551.
  - [17] V. Berezhinsky, V. Dokuchaev, and Y. Eroshenko, Phys. Rev. D **73**, 063504 (2006), arXiv:astro-ph/0511494.
  - [18] L. Pieri, G. Bertone, and E. Branchini, Mon. Not. R. Astron. Soc. **384**, 1627 (2008), arXiv:0706.2101.
  - [19] J. Lavalle, J. Pochon, P. Salati, and R. Taillet, Astron. & Astrophys. **462**, 827 (2007).
  - [20] J. Lavalle, Q. Yuan, D. Maurin, and X.-J. Bi, Astron. & Astrophys. **479**, 427 (2008), arXiv:0709.3634.
  - [21] F. Donato, N. Fornengo, D. Maurin, P. Salati, and R. Taillet, Phys. Rev. D **69**, 063501 (2004).
  - [22] A. M. Lionetto, A. Morselli, and V. Zdravkovic, Journal of Cosmology and Astro-Particle Physics **9**, 10 (2005).
  - [23] T. Delahaye, R. Lineros, F. Donato, N. Fornengo, and P. Salati, ArXiv e-prints **712** (2007), 0712.2312.
  - [24] J. Diemand, M. Kuhlen, P. Madau, M. Zemp, B. Moore, D. Potter, and J. Stadel, ArXiv e-prints **805** (2008), 0805.1244.
  - [25] R. Teyssier, Astron. & Astrophys. **385**, 337 (2002), arXiv:astro-ph/0111367.
  - [26] S. Casertano and P. Hut, Astrophys. J. **298**, 80 (1985).
  - [27] T. Delahaye, J. Lavalle, R. Lineros, P. Salati, F. Donato, N. Fornengo, and R. Taillet, in preparation (2008).
  - [28] F. Donato, D. Maurin, P. Salati, A. Barrau, G. Boudoul, and R. Taillet, Astrophys. J. **563**, 172 (2001).
  - [29] A. W. Strong and I. V. Moskalenko, Astrophys. J. **509**, 212 (1998), arXiv:astro-ph/9807150.
  - [30] V. S. Berezhinskii, S. V. Bulanov, V. A. Dogiel, and V. S. Ptuskin, *Astrophysics of cosmic rays* (Amsterdam: North-Holland, 1990, edited by Ginzburg, V.L., 1990).
  - [31] D. Maurin, F. Donato, R. Taillet, and P. Salati, Astrophys. J. **555**, 585 (2001).
  - [32] D. Maurin, R. Taillet, and F. Donato, Astronomy and Astrophys. **394**, 1039 (2002).
  - [33] F. Donato, D. Maurin, and R. Taillet, Astronomy and Astrophys. **381**, 539 (2002).
  - [34] J. S. Perko, Astron. & Astrophys. **184**, 119 (1987).
  - [35] D. Maurin, R. Taillet, F. Donato, P. Salati, A. Barrau, and G. Boudoul, Research Signposts, Recent Research Developments in Astronomy and Astrophys. **2**, 193 (astro-ph/021211) (2004), astro-ph/0212111.
  - [36] A. Barrau, G. Boudoul, F. Donato, D. Maurin, P. Salati, and R. Taillet, Astron. & Astrophys. **388**, 676 (2002), arXiv:astro-ph/0112486.
  - [37] A. Barrau, P. Salati, G. Servant, F. Donato, J. Grain, D. Maurin, and R. Taillet, Phys. Rev. D **72**, 063507



- (2005).
- [38] T. Bringmann and P. Salati, *Phys. Rev. D* **75**, 083006 (2007).
  - [39] E. A. Baltz and J. Edsjö, *Phys. Rev. D* **59**, 023511 (1999), [astro-ph/9808243](#).
  - [40] P. Brun, G. Bertone, J. Lavalle, P. Salati, and R. Taillet, *Phys. Rev. D* **76**, 083506 (2007), [arXiv:0704.2543](#).
  - [41] R. Taillet and D. Maurin, *Astron. & Astrophys.* **402**, 971 (2003), [astro-ph/0212112](#).
  - [42] T. Sjöstrand, S. Mrenna, and P. Skands, *Journal of High Energy Physics* **5**, 26 (2006), [arXiv:hep-ph/0603175](#).
  - [43] G. Bélanger, F. Boudjema, A. Pukhov, and A. Semenov, *Computer Physics Communications* **174**, 577 (2006), [arXiv:hep-ph/0405253](#).
  - [44] P. Fayet and S. Ferrara, *Phys. Rept.* **32**, 249 (1977).
  - [45] H. E. Haber and G. L. Kane, *Phys. Rept.* **117**, 75 (1985).
  - [46] J. Ellis, D. V. Nanopoulos, and K. Tamvakis, *Physics Letters B* **121**, 123 (1983).
  - [47] G. L. Kane, C. Kolda, L. Roszkowski, and J. D. Wells, *Phys. Rev. D* **49**, 6173 (1994), [arXiv:hep-ph/9312272](#).
  - [48] A. Bottino, F. Donato, N. Fornengo, and P. Salati, *Phys. Rev. D* **58**, 123503 (1998), [arXiv:astro-ph/9804137](#).
  - [49] L. Bergström, J. Edsjö, and P. Ullio, *Astrophys. J.* **526**, 215 (1999), [arXiv:astro-ph/9902012](#).
  - [50] B. C. Allanach, M. Battaglia, G. A. Blair, M. Carena, A. de Roeck, A. Dedes, A. Djouadi, D. Gerdes, N. Ghodbane, J. Guion, et al., *European Physical Journal C* **25**, 113 (2002), [arXiv:hep-ph/0202233](#).
  - [51] A. Bottino, F. Donato, N. Fornengo, and P. Salati, *Phys. Rev. D* **72**, 083518 (2005), [arXiv:hep-ph/0507086](#).
  - [52] A. Bottino, N. Fornengo, G. Polesello, and S. Scopel, *Phys. Rev. D* **77**, 115026 (2008), [arXiv:0801.3334](#).
  - [53] T. Appelquist, H.-C. Cheng, and B. A. Dobrescu, *Phys. Rev. D* **64**, 035002 (2001), [arXiv:hep-ph/0012100](#).
  - [54] L. Randall and R. Sundrum, *Physical Review Letters* **83**, 4690 (1999), [arXiv:hep-th/9906064](#).
  - [55] L. Randall and R. Sundrum, *Physical Review Letters* **83**, 3370 (1999), [arXiv:hep-ph/9905221](#).
  - [56] G. Servant and T. M. P. Tait, *Nuclear Physics B* **650**, 391 (2003), [arXiv:hep-ph/0206071](#).
  - [57] G. Bertone, G. Servant, and G. Sigl, *Phys. Rev. D* **68**, 044008 (2003), [arXiv:hep-ph/0211342](#).
  - [58] K. Agashe and G. Servant, *Physical Review Letters* **93**, 231805 (2004), [arXiv:hep-ph/0403143](#).
  - [59] K. Agashe and G. Servant, *Journal of Cosmology and Astro-Particle Physics* **2**, 2 (2005), [arXiv:hep-ph/0411254](#).
  - [60] D. Hooper and G. Servant, *Astroparticle Physics* **24**, 231 (2005), [arXiv:hep-ph/0502247](#).
  - [61] R. Barbieri, L. J. Hall, and V. S. Rychkov, *Phys. Rev. D* **74**, 015007 (2006), [hep-ph/0603188](#).
  - [62] L. Lopez Honorez, E. Nezri, J. F. Oliver, and M. H. G. Tytgat, *JCAP* **0702**, 028 (2007), [hep-ph/0612275](#).
  - [63] N. Arkani-Hamed, A. G. Cohen, and H. Georgi, *Phys. Lett. B* **513**, 232 (2001), [hep-ph/0105239](#).
  - [64] M. Schmaltz and D. Tucker-Smith, *Ann. Rev. Nucl. Part. Sci.* **55**, 229 (2005), [arXiv:hep-ph/0502182](#).
  - [65] H.-C. Cheng and I. Low, *JHEP* **09**, 051 (2003), [arXiv:hep-ph/0308199](#).
  - [66] T. Han, H. E. Logan, B. McElrath, and L.-T. Wang, *Phys. Rev. D* **67**, 095004 (2003), [arXiv:hep-ph/0301040](#).
  - [67] A. Birkedal, A. Noble, M. Perelstein, and A. Spray, *Phys. Rev. D* **74**, 035002 (2006), [arXiv:hep-ph/0603077](#).
  - [68] M. Asano, S. Matsumoto, N. Okada, and Y. Okada, *Phys. Rev. D* **75**, 063506 (2007), [arXiv:hep-ph/0602157](#).
  - [69] W. Dehnen, in *Disks of Galaxies: Kinematics, Dynamics and Perturbations*, edited by E. Athanassoula, A. Bosma, and R. Mújica (2002), vol. 275 of *Astronomical Society of the Pacific Conference Series*, pp. 105–116.
  - [70] N. Bissantz and O. Gerhard, *Mon. Not. R. Astron. Soc.* **330**, 591 (2002), [arXiv:astro-ph/0110368](#).
  - [71] E. Athanassoula, *Mon. Not. R. Astron. Soc.* p. 339 (2007), [arXiv:astro-ph/0703184](#).
  - [72] E. Athanassoula, F.-S. Ling, and E. Nezri, *Phys. Rev. D* **72**, 083503 (2005), [astro-ph/0504631](#).
  - [73] M. Boezio, P. Carlson, T. Francke, N. Weber, M. Suffert, M. Hof, W. Menn, M. Simon, S. A. Stephens, R. Bellotti, et al., *Astrophys. J.* **532**, 653 (2000).
  - [74] M. A. DuVernois, S. W. Barwick, J. J. Beatty, A. Bhattacharyya, C. R. Bower, C. J. Chaput, S. Coutu, G. A. de Nolfo, D. M. Lowder, S. McKee, et al., *Astrophys. J.* **559**, 296 (2001).
  - [75] M. Aguilar et al. (AMS), *Phys. Rept.* **366**, 331 (2002).
  - [76] S. Orito, T. Maeno, H. Matsunaga, K. Abe, K. Anraku, Y. Asaoka, M. Fujikawa, M. Imori, M. Ishino, Y. Makida, et al., *Physical Review Letters* **84**, 1078 (2000), [arXiv:astro-ph/9906426](#).
  - [77] T. Maeno, S. Orito, H. Matsunaga, K. Abe, K. Anraku, Y. Asaoka, M. Fujikawa, M. Imori, Y. Makida, N. Matsui, et al., *Astroparticle Physics* **16**, 121 (2001), [arXiv:astro-ph/0010381](#).
  - [78] Y. Asaoka, Y. Shikaze, K. Abe, K. Anraku, M. Fujikawa, H. Fuke, S. Haino, M. Imori, K. Izumi, T. Maeno, et al., *Physical Review Letters* **88**, 051101 (2002), [arXiv:astro-ph/0109007](#).
  - [79] S. Haino and et al., in *International Cosmic Ray Conference* (2005), vol. 3 of *International Cosmic Ray Conference*, pp. 13–+.
  - [80] J. S. Bullock, T. S. Kolatt, Y. Sigad, R. S. Somerville, A. V. Kravtsov, A. A. Klypin, J. R. Primack, and A. Dekel, *Mon. Not. R. Astron. Soc.* **321**, 559 (2001), [astro-ph/9908159](#).
  - [81] J. Diemand, M. Kuhlen, and P. Madau, *Astrophys. J.* **667**, 859 (2007), [arXiv:astro-ph/0703337](#).
  - [82] M. Casolino, P. Picozza, F. Altamura, A. Basili, N. De Simone, V. Di Felice, M. P. De Pascale, L. Marcelli, M. Minori, M. Nagni, et al., *ArXiv e-prints* **arXiv:0708.1808** (2007), 0708.1808.
  - [83] A. A. Moiseev, J. F. Ormes, and I. V. Moskalenko, *ArXiv e-prints* **706** (2007), 0706.0882.
  - [84] J. Diemand, B. Moore, and J. Stadel, *Nature (London)* **433**, 389 (2005), [astro-ph/0501589](#).
  - [85] G. Gentile, P. Salucci, U. Klein, D. Vergani, and P. Kalberla, *Mon. Not. R. Astron. Soc.* **351**, 903 (2004), [arXiv:astro-ph/0403154](#).
  - [86] P. Englmaier and O. Gerhard, *Celestial Mechanics and Dynamical Astronomy* **94**, 369 (2006), [arXiv:astro-ph/0601679](#).